Research Article

Analytical Study of Geometric Parameter Effect on the Behavior of Horizontally Curved Reinforced Concrete Deep Beam

Goshu Kenea [ID]

Department of Civil Engineering, Faculty of Civil and Environmental Engineering, Jimma Institute of Technology, Jimma University, Jimma, Oromia, Ethiopia

Correspondence should be addressed to Goshu Kenea; goshukeneatujuba@gmail.com

Nonlinear finite element simulation was once employed to look into the behavior of horizontally curved reinforced concrete deep beams under concentrated load at its mid-span. The study focused on the parametric impact of span length-to-depth (L/D) and span length-to-radius (L/R) ratios. In addition, the effect of longitudinal and spacing of shear reinforcement on the behavior of the beam has been investigated. The study considered sixteen beam specimens. Three of these specimens were straight beams as a control, and others were curved beams. The concrete-damaged plasticity model has been used to model the beam with C-25 grade concrete and steel reinforcements having diameters of $\varnothing$ 4 mm, $\varnothing$ 10 mm, and $\varnothing$ 12 mm with 568 MPa, 596 MPa, and 643 MPa steel grade, respectively. Reduced twenty-noded brick (C3D20 R) and two-noded (T3D2) elements have been used for modeling concrete and steel, respectively. The ultimate load capacity, the strain distribution, the load-deflection curve, and the load-twisting curve are the main outputs of the FE simulation. The study confirmed a considerable decrease in load-carrying capacity by up to 8.74% and 27.95% as the (L/R) ratio increased from 0 to 1.57 and the L/D ratio increased from 2.4 to 3, respectively. However, as the longitudinal steel ratio increased from 0.02042 to 0.02608 and the spacing of shear reinforcement decreased from 100 mm to 50 mm, the ultimate load capacity is increased up to 9.28% and 4.3%, respectively. Sensitivity evaluation was also conducted to see how much the independent variables (L/D ratio, L/R ratio, longitudinal bar ratio, and spacing transverse reinforcement) affect the dependent parameter (ultimate load capacity).

1. Introduction

Horizontally curved reinforced concrete beams are extensively used in many fields, such as in the construction of modern highway bridges, circular balconies, rounded corners of buildings, and stadium construction. Curved beams with higher depth are required to resist huge loads and to fulfill some aesthetic purposes. Deep beams are structural members having a larger depth than shallow beams, and the thickness is much smaller than either depth or span [1]. The deep beam is defined differently as per different codes. The beam is classified as a deep beam when the magnitude relation of its effective span length L to overall depth D is smaller than 2, and 2.5 for simply supported and continuous beams, respectively [2]. In another way, when the beams have either clear spans, equal to or less than four times the overall member depth, or regions with concentrated loads within twice the member depth from the face of the support, it is considered a deep beam according to [3], and as span length to overall depth is less than or equal to 3, it is considered to be deep beams based on [4]. They dissent from shallow beams within the sense that strain distribution across the depth is nonlinear and cannot delineate in terms of uniaxial stress-strain characteristics [5, 6]. Moreover, the nonhomogeneous nature of the materials concerned contributes to the complexness of the matter. Therefore, it becomes necessary to use advanced numerical analysis procedures to satisfy the safety and economic necessities during the design of structures.

Different methods are available for analyzing deep beams. The strut and tie model (STM) provides structural engineers with a lot of versatile and intuitive possibilities for

coming up with structural elements [7, 8]. However, it is difficult to identify optimum truss configuration because of its complexness and the inability to predict failure mode. As a result, it is not widely used [9]. A finite element method is a good tool for its realistic and satisfactory solutions for the nonlinearity behavior of reinforced concrete deep beams [10–12]. Using this method allows exactly investigating different behavior of concrete members. These aspects include the tension-stiffening, nonlinearity multi-axial material properties, modeling of cracking and crushing under loads, and many other properties related to the behavior of reinforced concrete members under stress. The utilization of finite element methodology contains modeling of the degradation of concrete compressive strength with transverse tensile strain happens in members subjected dominantly to torsion and shear stresses. During this study, the damaged plasticity model, as stated within the general-purpose finite element package [13], is employed to review the behavior of beams. This constitutional modeling is supported with evidence to be the foremost stable regime for modeling concrete nonlinear behavior. It shows the flexibility to capture the total concrete behavior up to failure with reliable accuracy compared to the experimental results [14–18].

Currently, the demand is increasing for constructing different types of structures to resist different types of loading, both dynamic and static loading. A deep beam is one type and can be made with several forms and arrangements to extend its resistance to torsion, shear, bending moment, fire, and temperature and to suit the geometric pattern of the building structure. Traditional-style assumptions concerning section stay plane after bending for shallow beams did not apply to deep beams [19]. However, it ought to note existing codes of practices have not adequately addressed the behavior of deep beams particularly, horizontally curved-deep beams. Most of the studies performed antecedently primarily targeted the behavior of horizontally straight deep beams with and without opening [6, 20–25]. However, an investigation has been conducted on the behavior of curved-deep beams on the Winkler foundation using the finite difference method [19]. In a general sense, the studies performed on the horizontally curved reinforced concrete deep beam are rare. The failure behavior of deep beams is different from that of shallow beams due to geometry and load transfer mechanism. In addition, the serviceability and failure pattern are not reported of those structural parts extensively due to the shortage of clear procedures for the prediction of its behavior.

Therefore, a detailed study of load-carrying capacity, shear, moment, and torsional behavior of reinforced concrete deep beam is required to provide a safe and economic structure [19]. There arises the need for more elaborate investigations for better understanding and design of deep beams. The study has adopted a three-dimensional finite element model and aimed at investigating the behavior of the beams. The focus is to assess the effect of geometric parameter ratios (L/D & L/R), longitudinal steel ratio, and stirrups spacing on strain distribution, load-deflection response, load-twisting response, and load-carrying capacity of the deep beams.

2. Materials and Methods

2.1. Material Modeling

2.1.1. Concrete. Compressive Stress-Strain. The stress-strain data for concrete are crucial for analysis utilizing the concrete-damaged plasticity model. However, the experimental results have not been reported yet, and only the ultimate compressive strength of the concrete at 28 days was used. Concrete with C-25 MPa was used. Stress-strain data input is extracted using Eurocode 2 [20] mathematical model provision. Concrete behaves linearly within the elastic region until $\sigma_{co} = 0.4\sigma_{cu}$, *where,* $\sigma_{cu} = f_c' = f_{cm}$. In this circumstance, the value of 0.0022 and 0.0035 was taken at peak and the nominal ultimate strain, respectively. After reaching this point, concrete starts to undergo in a plastic fashion and exhibits some work-hardening up to the ultimate stress, σ_{cu}, followed by strain-softening. Different parameters defining the concrete-damaged plasticity model were computed as proposed in [21–23]. Isotropic damaged elasticity in tension and compression was employed to present the inelastic behavior of concrete.

Tensile Stress-Strain. The concrete tensile stress-strain behavior under uniaxial tensile loading was used for this particular study. The tensile stress-strain has been used as input to model concrete in the concrete-damaged plasticity model. The relationship is linear elastic until the peak point, and then, it induces a strain-softening postpeak response [13]. The equations proposed in a paper [20, 24] were used to extract the tensile stress-strain of concrete.

Selection Of Concrete Damage Parameters. Since the calculations for these parameters involve complex mathematical derivations and assumptions using the yield surface of the concrete-damaged plasticity model, the proposed values in other researchers' work have been used here [25–30]. The verification was checked by comparing the numerical results with published experimental data. Table 1 presents the concrete damage parameter of the study. Table 2 illustrates the summary of concrete properties used for the modeling.

2.1.2. Steel. Steel is assumed to be an elastoplastic material and identical in tension and compression with a linear elastic response up to yield point and hardening stress from yield point to the ultimate strain. The study used the steel reinforcement with a Poisson ratio of 0.3 and an elastic modulus of 200,000 MPa, and 2.5% of the elastic modulus was used for the hardening modulus of elasticity [31]. Table 3 illustrates the summary of steel properties and its diameter used for the model.

2.2. Geometry. Different parts were modeled to cover the objectives of the study with the FE simulation software package. These parts include concrete plain beam, and longitudinal and shear reinforcement. Based on independent variables, sixteen numbers of the sample were considered in the study. Length-depth ratio, length-radius ratio, longitudinal steel ratio, and stirrups spacing were the main study parameters in the model. Table 4 illustrates the geometric

TABLE 1: Concrete damage parameter.

Eccentricity (γ)	Dilation angle (ψ)	K	σ_{bo}/σ_{co}	Viscosity parameter
0.1	31	0.667	1.16	0.0001

TABLE 2: Concrete properties [16].

Concrete properties	Elastic modulus (MPa)	Poisson's ratio	Compressive strength (MPa)	Tensile strength
Magnitude	28960	0.2	25	1.923a

TABLE 3: Diameter and properties of steel reinforcements.

No	Diameter (mm)	Elastic region		Inelastic regions	Elastic modulus (GPa)
		f_y (MPa)	ε_y (%)	f_u (MPa)	
1	4	568	0.2840	596.40	200
2	10	596	0.2980	625.80	200
3	12	643	0.3215	675.15	200

TABLE 4: The case understudied and the dimension of the deep beams model.

| No	Beam ID	Length (mm)	Depth (mm)	Width (mm)	L/R ratio	L/D ratio	Long. bar size (mm)	Stirrup size (mm)
1	DB10	1200	400	100	—	3	4Φ4, 4Φ10, & 4Φ12	Φ4c/c100
2	DB11	1200	400	100	1.05	3	4Φ4, 4Φ10, & 4Φ12	Φ4c/c100
3	DB12	1200	400	100	1.31	3	4Φ4, 4Φ10, & 4Φ12	Φ4c/c100
4	DB13	1200	400	100	1.57	3	4Φ4, 4Φ10, & 4Φ12	Φ4c/c100
5	DB20	1200	450	100	—	2.67	4Φ4, 4Φ10, & 5Φ12	Φ4c/c100
6	DB21	1200	450	100	1.05	2.67	4Φ4, 4Φ10, & 5Φ12	Φ4c/c100
7	DB22	1200	450	100	1.31	2.67	4Φ4, 4Φ10, & 5Φ12	Φ4c/c100
8	DB23	1200	450	100	1.57	2.67	4Φ4, 4Φ10, & 5Φ12	Φ4c/c100
9	DB30	1200	500	100	—	2.4	4Φ4, 4Φ10, & 6Φ12	Φ4c/c100
10	DB31	1200	500	100	1.05	2.4	4Φ4, 4Φ10, & 6Φ12	Φ4c/c100
11	DB32	1200	500	100	1.31	2.4	4Φ4, 4Φ10, & 6Φ12	Φ4c/c100
12	DB33	1200	500	100	1.57	2.4	4Φ4, 4Φ10, & 6Φ12	Φ4c/c100
13	DB11-L	1200	400	100	1.05	3	4Φ4, 4Φ10, & 6Φ12	Φ4c/c100
14	DB13-L	1200	400	100	1.57	3	4Φ4, 4Φ10, & 6Φ12	Φ4c/c100
15	DB11-S	1200	400	100	1.05	3	4Φ4, 4Φ10, & 4Φ12	Φ4c/c50
16	DB13-S	1200	400	100	1.57	3	4Φ4, 4Φ10, & 4Φ12	Φ4c/c50

(a) (b) (c) (d)
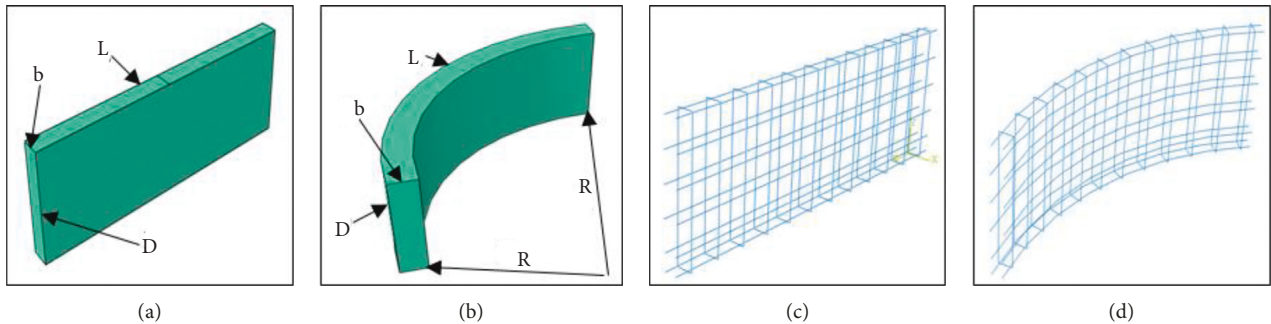
FIGURE 1: Sample geometric description of the deep beam and steel reinforcement. (a) Straight concrete plain beam, (b) curved concrete plain beam, (c) detailing for straight beam, and (d) detailing for curved beam.

dimension and number of the deep beams used for modeling in finite element software Abaqus/CAE, to cover the required objective. Figure 1 shows the geometric description of sample deep beams including detailed reinforcement for modeling. Figure 2 indicates the geometric cross section of the beams.
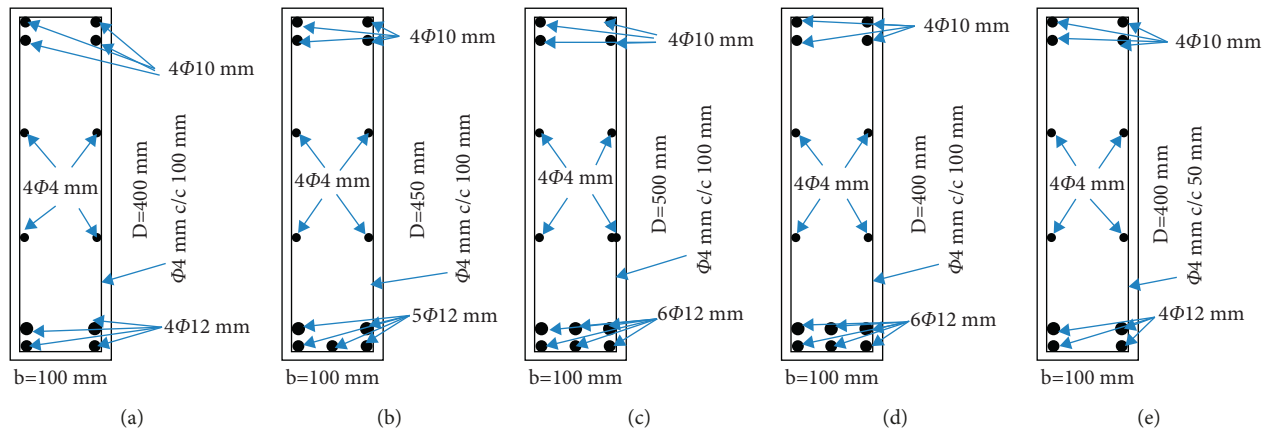
FIGURE 2: Cross-sectional view of deep beam specimens (a) DB10, DB11, DB12, & DB13, (b) DB20, DB21, DB22, & DB23, (c) DB30, DB31, DB32, & DB33, (d) DB11-L & DB13-L, and (e) DB11-S & DB13-S.

2.3. Element Type and Meshing. Quadratic reduced solid 3D with twenty-noded brick (C3D20 R) and node linear 3D truss element (T3D2) have been used to model concrete and steel reinforcement, respectively. Figure 3(a) shows the meshing type employed during analysis. A 25 mm mesh size has been employed for all models.

2.4. Loading and Boundary Condition. Fixed end support has been considered to model the boundary conditions of the specimens. The static concentrated load has been applied at the mid-span of the beam until it reaches ultimate capacity. Figure 3(b) shows the loading and boundary conditions of the beams.

2.5. Validation of FE Model. The researchers [32] conducted experimental investigations on horizontally curved reinforced concrete beams, which is used as validation of the FE simulation of this study. The beam is curved in a circular arc with subtending an angle of 86 degrees. Single concentrate load was used to investigate the behavior of the test specimen. Figure 4 illustrates geometry, detailing reinforcement, boundary condition, and loading condition of the test specimen. The material properties presented in Table 5 were employed in modeling the beam specimen, based on test data. The theoretical results obtained from the finite element analysis showed a good agreement with the experimental values with a difference of 1.12% and 6% for ultimate loading and deflection, respectively. Figure 5 presents the comparison of experimental and finite element results. Concrete and steel properties that were used in the experimental investigation were applied in modeling FE of this study.

3. Result and Discussion

3.1. Strain Distribution

3.1.1. Concrete. In the reinforced concrete deep beam unlike normal reinforced beam, the stress-strain distribution is nonlinear across the cross section. To evaluate the strain distribution in the concrete section, the reading was taken

along the height of the section at the mid-span of the beam from the FE simulation of Abaqus software. Since the strain distribution of all deep beam specimens is similar, one deep beam specimen (DB-12) was taken as a sample. Figure 6 presents the strain distribution in the concrete section at the cracking and the ultimate stage of loading at the mid-span and near support of the beam. There is a slight variation of neutral axis position at cracking and ultimate loading for both near support and at mid-span. The slope of strain versus section height curve is significantly affected when the comparison is undertaken between cracking and ultimate loading. The slope of the curve is flatter at ultimate loading than at cracking loading for both positions: near support and mid-span.

3.1.2. Steel Reinforcement. In addition to strain distribution in the concrete section, the strain distribution in longitudinal reinforcement has been investigated along the length of the deep beam for both negative and positive reinforcement. Figure 7 shows the strain distribution in the longitudinal reinforcement along the length of the beam at a different stage (at cracking and ultimate) of loading for both negative and positive reinforcement of the DB-12 beam specimen, respectively. The strain in the reinforcement along the length is compression in some portions and tension in some portions. This is mainly caused due to fixed end support condition of the beam. Fixed end support results in tension at top fiber and compression at bottom fiber at near support and tension at bottom fiber and compression at top fiber at mid-span of the beam, which is different from simply supported deep beam. The strain distribution of one specimen (DB-12) was shown since the strain distribution is almost the same for all specimens. Each longitudinal reinforcement is subjected to both tension and compression stress along its length, which is caused by the fixed support condition of the deep beam. Bottom reinforcements are subjected to compression and tension stress at near support and around mid-span, respectively. In another way, top reinforcements are subjected to compression and tension stress around mid-span and at near support, respectively
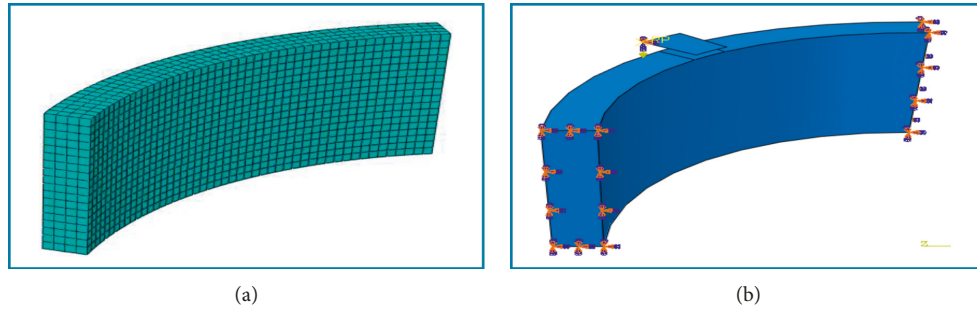
(a)

(b)

FIGURE 3: (a) Meshing and (b) loading boundary condition.

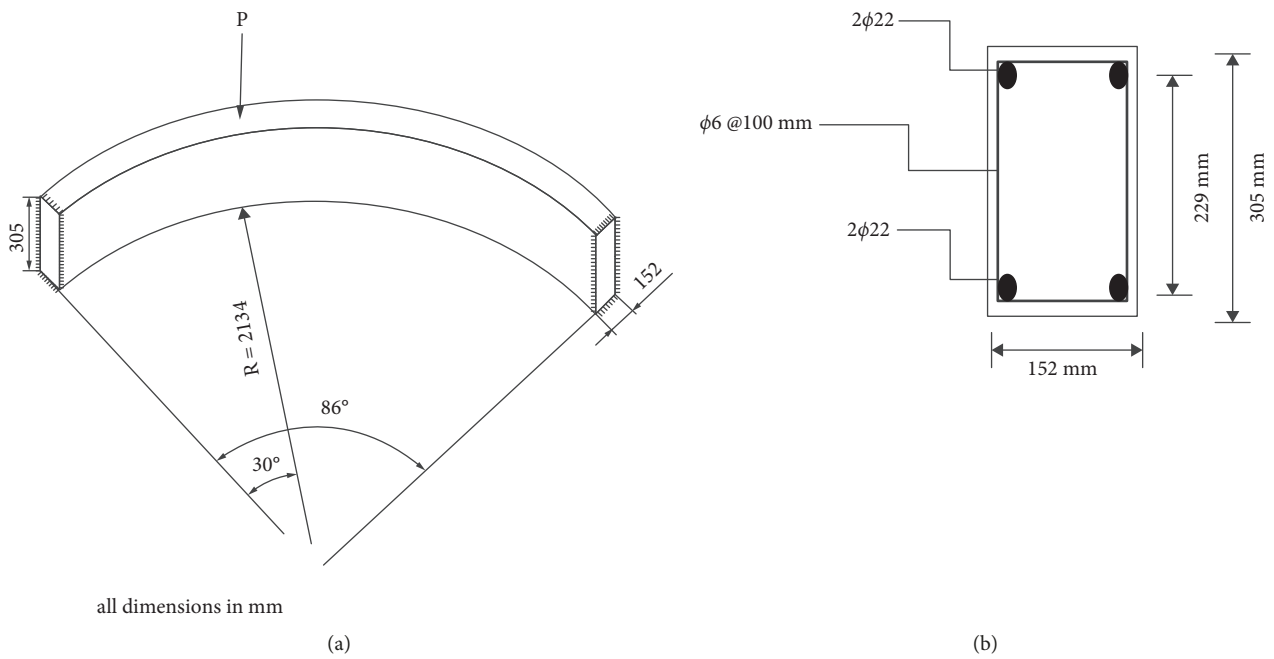all dimensions in mm

(a)

(b)

FIGURE 4: Curved RC beam test specimen for FE simulation validation [32]. (a) Geometric dimension of test specimen and (b) cross-sectional dimension with detailing.

TABLE 5: Material properties of test specimen used for FE simulation [32].

Concrete		Steel		
			Longitudinal bars	Stirrups
E (MPa)	29725			
f'c (MPa)	40	Es (MPa)	200000	200000
Ft (MPa)	3	Fy (MPa)	384	240
Poisson ratio	0.2	Poisson ratio	0.3	0.3

3.2. Load Deflection Curve. The load-deflection responses were extracted from the FE simulation at the mid-span of the beam to evaluate the effect of the L/D ratio, L/R ratio, longitudinal steel ratio, and vertical reinforcement spacing. Figure 8 presents the effect of the L/D ratio on the load-deflection response at the mid-span of the specimen. The curve shows that, as the L/D ratio of the deep beams increase, there is a significant decrease in the slope of the load-deflection curve under the same center of curvature. This implies that, at the same deflection, the load resisted by the lower L/D ratio is greater than the larger L/D ratio.

In addition, the load-deflection response presented from FE simulation to study the effect L/R ratio at the mid-span of the beams. Figure 9 shows the load-deflection curve of the beam at the mid-span under different L/R ratios by keeping the L/D ratio constant, which is used to access the effect of the L/R ratio on the load-displacement response curve of the beam. It is easily understood from the curve that the slope of the load-deflection curve is slightly decreased, as the L/R ratio of the beams increases, when compared to the L/D ratio effect. This shows at the same deflection the load resisted by the lower L/R ratio is larger than the larger L/R ratio. The
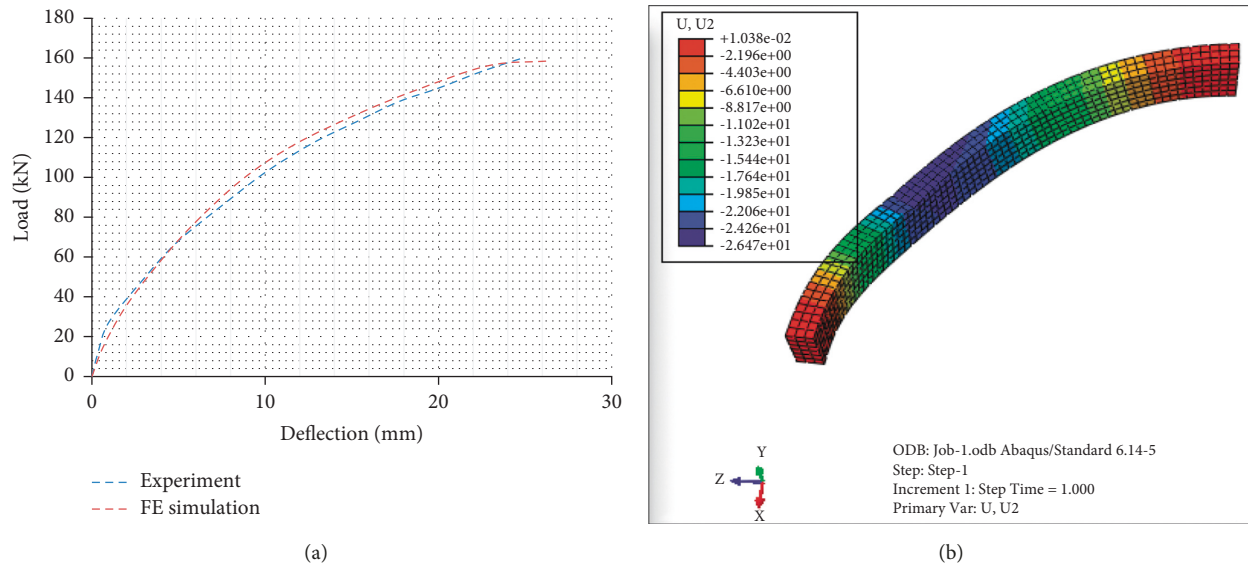
(a)

(b)

FIGURE 5: Comparison of FE and experimental result. (a) Load-deflection curve from experiment and FE analysis and (b) deformation response from FE analysis.
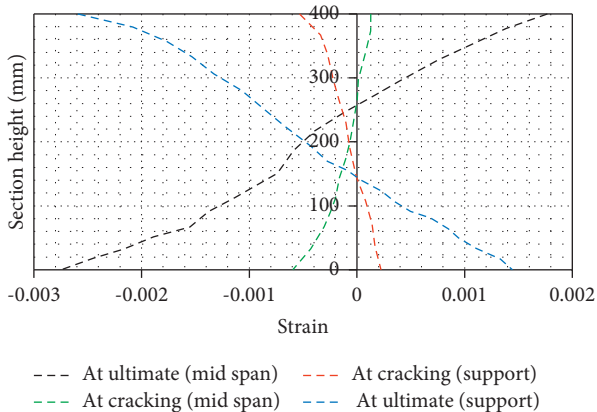

FIGURE 6: Strain distribution in the concrete section at support and mid-span.

decrease in load-carrying capacity/flexural capacity of the beam is caused due to the development of internal torsion, which is caused due to aspect ratio (L/R ratio). All specimens have constant length, but the different radius of curvature means different L/R ratios. Therefore, the decrease in load-carrying capacity is caused by the radius of curvature.

Furthermore, the load-deflection curve is presented in Figure 10 to access the effect of the longitudinal reinforcement ratio. The steel ratio has a significant effect on the load-deflection response curve. The slope of the curve is increased, as the longitudinal steel ratio increases. At the same loading condition, larger deflection occurs in the lower steel ratio specimen.

Furthermore, the shear reinforcement spacing was used as a study parameter, to see its effect on the load-deflection response of the beams. Figure 11 illustrates the load-deflection curve under different spacing vertical shear reinforcement with 100 mm and 50 mm center to center spacing.

The spacing of shear reinforcement has a significant effect on the curve because in a deep beam, shear force has a tremendous effect. Therefore, providing shear reinforcement decreases the effect that arises from the shear force on the load-carrying capacity of the specimen.

3.3. Load-Twisting Angle Curve. In addition to the load-deflection curve, the load-twisting angle curve has been determined using FE simulation results, to investigate the effect of L/D ratio, L/R ratio, longitudinal steel ratio, and shear reinforcement spacing. As it has been seen from Figure 12, the slope of the load-twisting angle significantly decreased, as the L/D ratio increased under the same aspect (L/R) ratio. On other hand, Figure 13 shows the load-twisting angle curve with different L/R ratios and the same L/D ratio. The slope of the curve is slightly decreased, as the L/R ratio increases. The decreasing slope of the load-twisting angle curve shows the increase in internal torsion in the beams due to the L/R ratio.

The load-twisting angle curve is also significantly affected by the longitudinal steel ratio and the spacing of shear reinforcement. Figure 14 shows the effect longitudinal reinforcement ratio considering other study parameters constant. The slope of the curve decreased, as the reinforcement ratio increased. This implies at the same deflection, a larger load is resisted by the larger steel ratio. In the same way, Figure 15 presents the load-twisting angle response under different spacing of shear reinforcement and keeping other parameters constant. The curve confirms the significance of shear reinforcement on the resistance of the beam. The study considered 100 mm and 50 mm center to center spacing of shear reinforcement. This implies under the same magnitude of loading, a larger twisting angle developed in the specimen with a lower longitudinal reinforcement ratio and larger shear spacing.
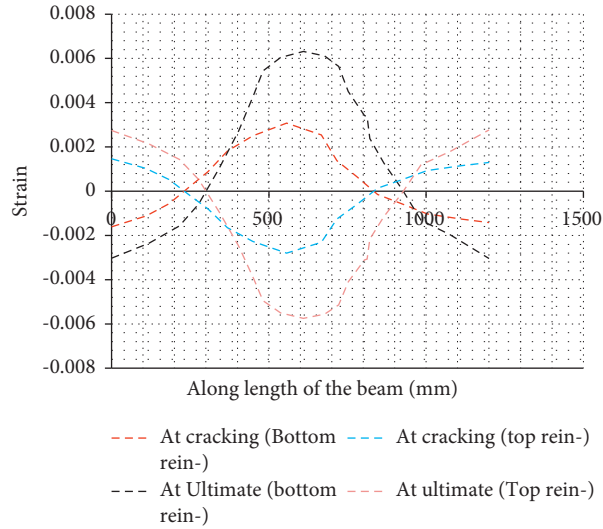
Figure 7: Strain distribution in the bottom and the top longitudinal steel reinforcement.

3.4. Ultimate Load Capacity. The ultimate load capacity of the beam is also another focus of the study extracted from FE simulation. Figures 16(a)–16(c) show the ultimate load capacity that was resisted by a deep beam having an L/D ratio of 3, 2.67, and 2.4, respectively, under different L/R ratios. This confirms that, as the L/D and L/R ratios increase, the ultimate load capacity is decreased. As the L/D ratio is increased from 2.4 to 2.67 and 2.4 to 3 the ultimate load capacity reduced by 14.51% and 27.95%, respectively. In other cases, as the L/R ratio was increased from 0 to 1.57 the ultimate load capacity reduced by 5.71%, 6.34%, and 8.74% for the beam specimen with L/D ratio equal to 3, 2.67, and 2.4, respectively. This shows that the ultimate load capacity is significantly affected by the L/D ratio when compared to the L/R ratio.

The ultimate load capacity of the beams is also significantly affected by shear reinforcement spacing and longitudinal steel reinforcement ratio. The load-carrying capacity generally increased, as the spacing of shear reinforcement decreased and longitudinal reinforcement ratio increased, as illustrated in Figures 17(a) and 17(b), respectively. As the longitudinal steel ratio increased from 0.02042 to 0.02608, the ultimate load capacity increased up to 9.28%. In other cases, as spacing shear reinforcement decreased from 100 mm to 50 mm for DB-11 and DB-13 specimens, the ultimate load capacity of the beam increased up to 4.3%. The analysis result testified that the longitudinal reinforcement ratio has a more significant effect on the load-carrying capacity of the beam, as compared to shear reinforcement spacing.

In general, the reduction of the load-carrying capacity of the deep beams with the same depth, width, length, and steel reinforcement is due to the variation of center of curvature, which mainly causes internal torsional moments in the beam. Table 6 summarizes the cracking load, ultimate load, ultimate deflection, and ultimate twisting angle for the whole specimens. The cracking loading is also significantly affected by the L/R ratio, L/D ratio, longitudinal reinforcement ratio, and shear reinforcement spacing. As the L/R increased from 0 to 1.57 and the L/D ratio increased from 2.4 to 3, the cracking loading of the model specimens is decreased up to 12.35%, and 26.17%, respectively. In addition, the cracking loading increased up to 12.30%, as the reinforcement ratio increased from 0.02042 to 0.02608. Furthermore, the study showed that, as vertical reinforcement spacing decreased from 100 mm to 50 mm, the cracking loading is increased up to 7.3%.

3.5. Sensitivity Analysis. Based on the result data obtained from FE simulation, sensitivity analysis was performed using rigorous multilinear regression in SPSS software. Equation (1) shows the empirical relationship between input parameters (L/D ratio, L/R ratio, longitudinal reinforcement steel ratio, and spacing of vertical shear reinforcement) and the ultimate load-carrying capacity of the beam. The equation shows a negative relationship between load-carrying capacity and geometric parameter ratio (L/D and L/R ratios) and spacing of shear reinforcement. However, the effect of the L/D ratio is more significant than the L/R ratio based on the coefficient of the parameters. On other hand, there is a positive relationship between load-carrying capacity and longitudinal reinforcement ratio. The negative coefficient shows that as the input value increases, the output value decreases and vice versa:

$$p_{ul} = -24.31r - 242.2\,d + 11517.7\rho - 0.79099s + 1001.003, \quad (1)$$

where p_{ul} is the beam ultimate load-carrying capacity (kN), r is L/R ratio (mm/mm), d is L/D ratio (mm/mm), ρ is longitudinal reinforcement ratio (A_s/bd), and s is spacing of vertical shear reinforcement (mm).
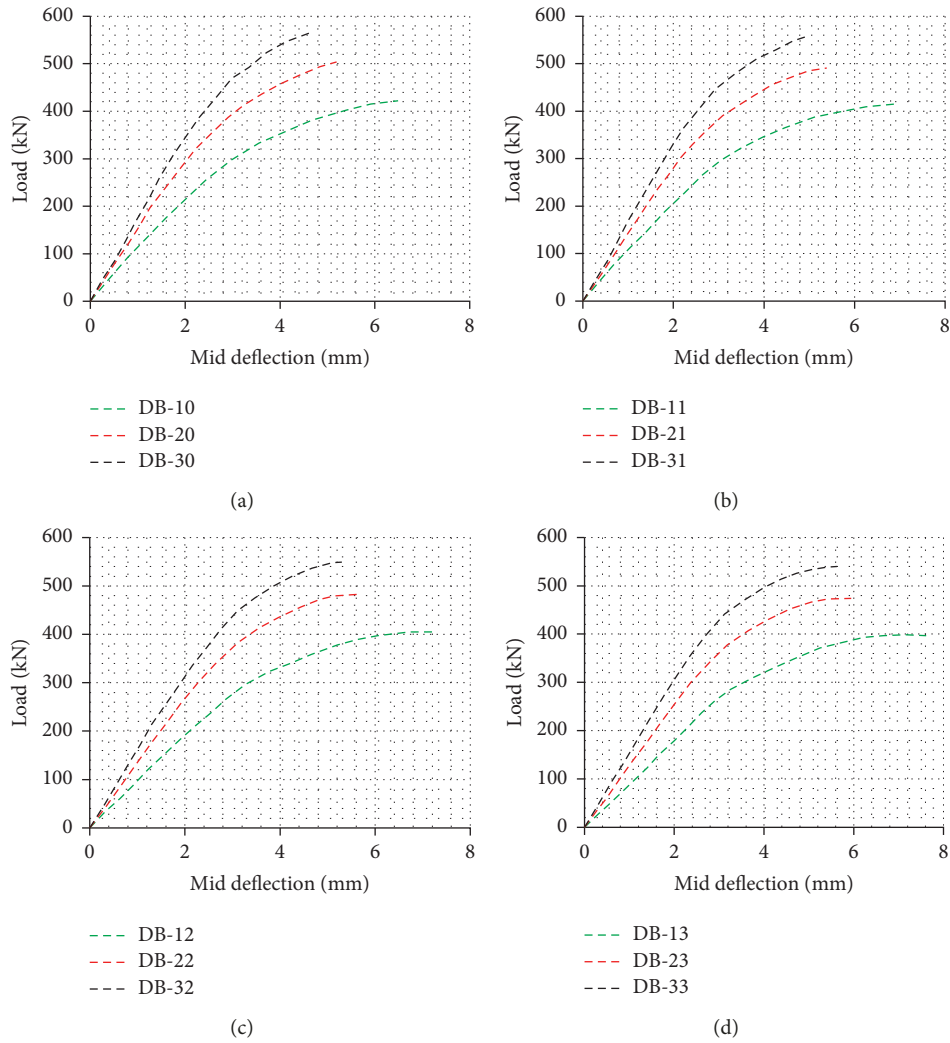
(a)

(b)

(c)

(d)

FIGURE 8: Load-deflection response curves with different L/D ratios of 3, 2.67, and 2.4. (a) Straight beam, (b) beam with L/R ratio equal to 1.05, (c) beam with L/R ratio equal to 1.31, and (d) beam with L/R ratio equal to 1.57.
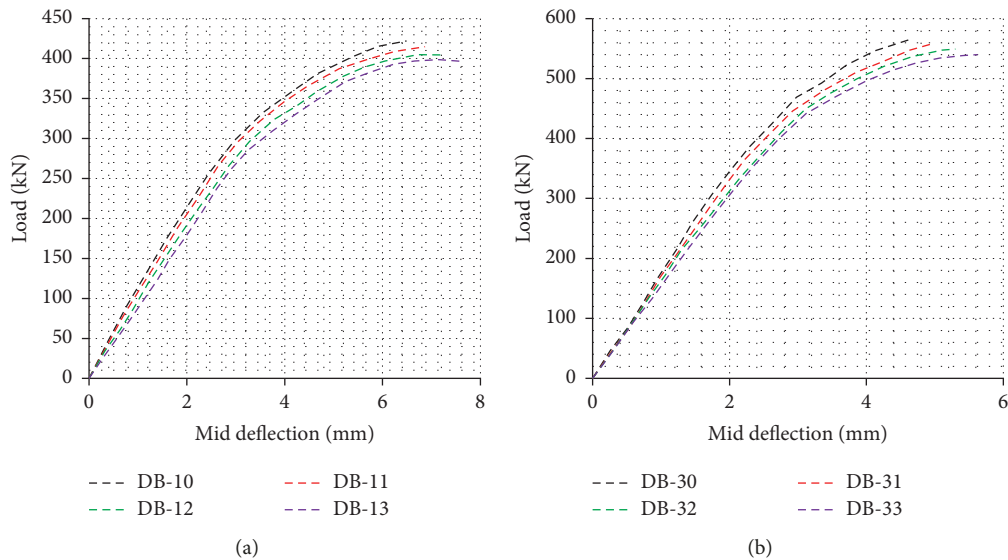

(a)

(b)

FIGURE 9: Load-deflection response curves with different L/R ratios of 0, 1.05, 1.31, and 1.57. (a) Beam with L/D ratio equal to 3, and (b) beam with L/D ratio equal to 2.4.
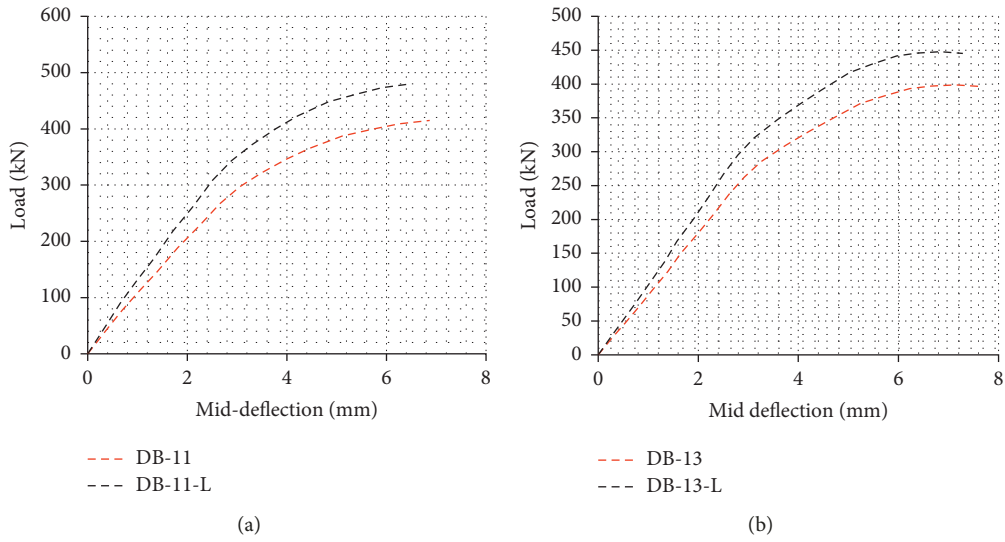
FIGURE 10: Load-deflection response curves with different longitudinal steel ratios of 0.02042 to 0.02608. (a) Beam with L/D and L/R ratios equal to 3 and 1.05, respectively, and (b) beam with L/D and L/R ratios equal to 3 and 1.57, respectively.
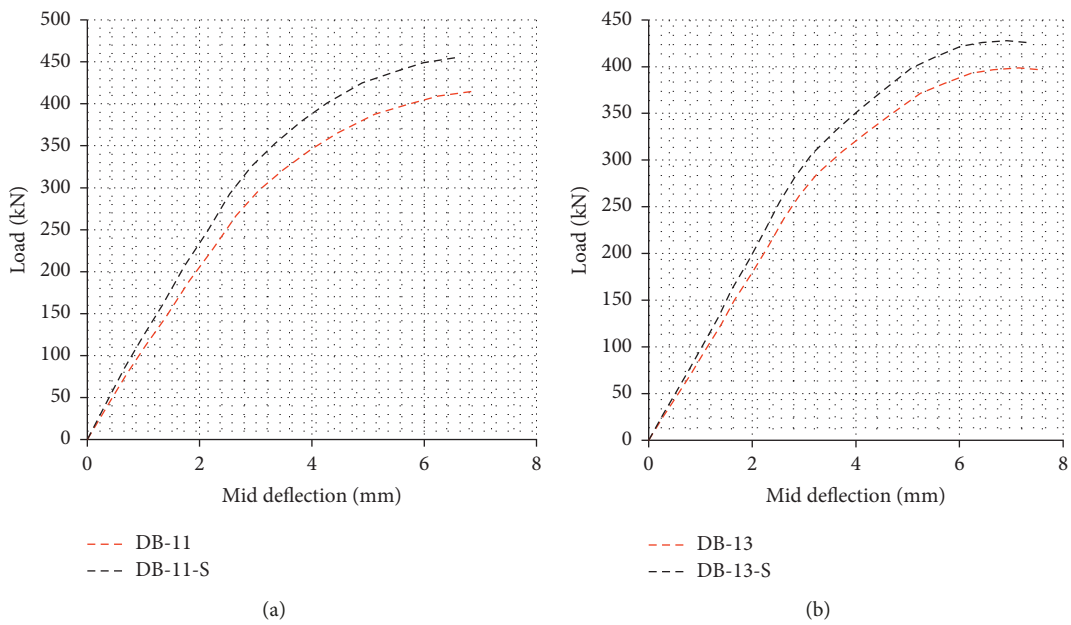

FIGURE 11: Load-deflection response curves with different spacing of stirrups (100 mm and 50 mm). (a) Beam with L/D and L/R ratios equal to 3 and 1.05, respectively, and (b) beam with L/D and L/R ratios equal to 3 and 1.57, respectively.
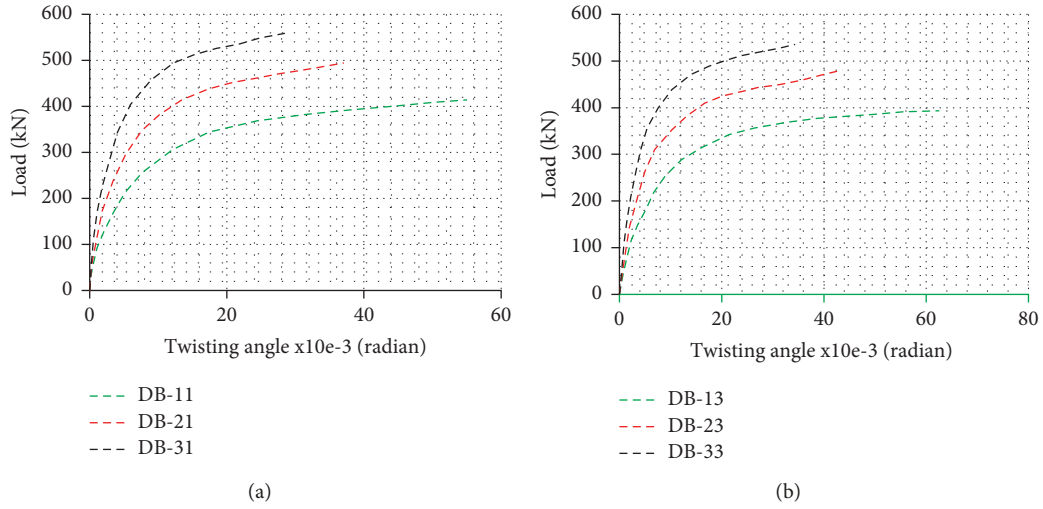
(a)

(b)

FIGURE 12: Load-rotation response curves with different L/D ratios of 3, 2.67, and 2.4. (a) Beam with L/R ratio equal to 1.05 and (b) beam with L/R ratio equal to 1.57.
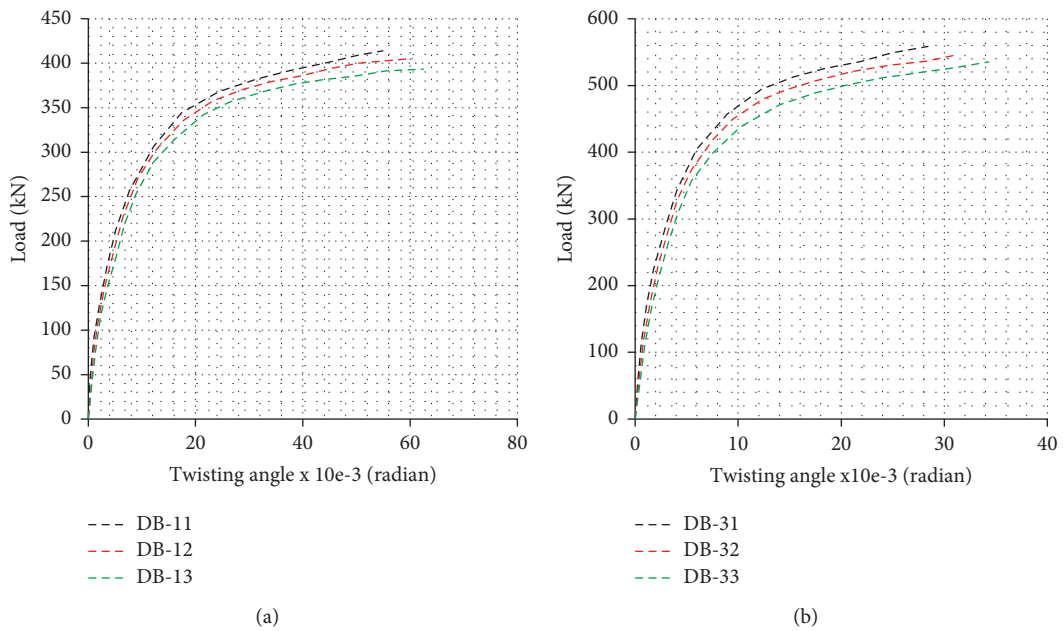

(a)

(b)

FIGURE 13: Load-rotation response curves with different L/R ratios of 1.05, 1.31, and 1.57. (a) Beam with L/D ratio equal to 3 and (b) beam with L/D ratio equal to 2.4.
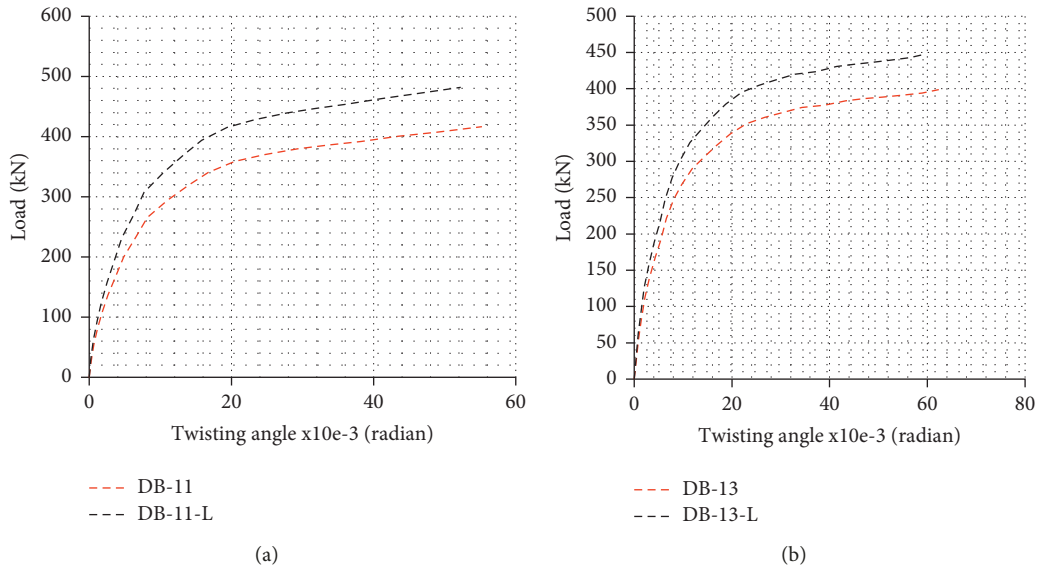
FIGURE 14: Load-rotation response curves with different longitudinal steel ratios of 0.0011 and 0.123. (a) Beam with L/D and L/R ratios equal to 3 and 1.05, respectively, and (b) beam with L/D and L/R ratios equal to 3 and 1.57, respectively.
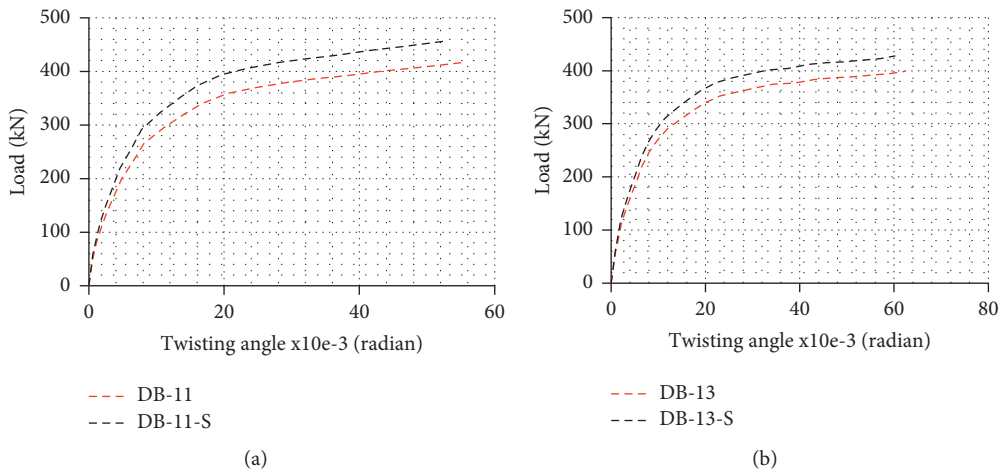

FIGURE 15: Load-twisting angle curves with different spacing of vertical shear reinforcement (100 mm and 50 mm). (a) Beam with L/D and L/R ratios equal to 3 and 1.05, respectively, and (b) beam with L/D and L/R ratios equal to 3 and 1.57, respectively.
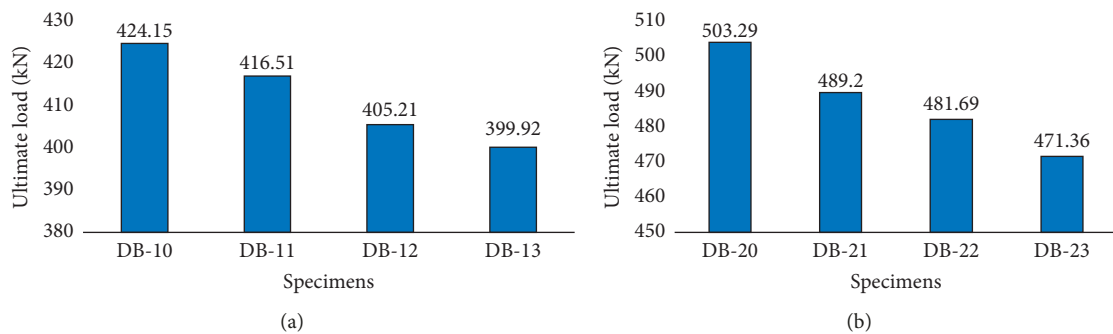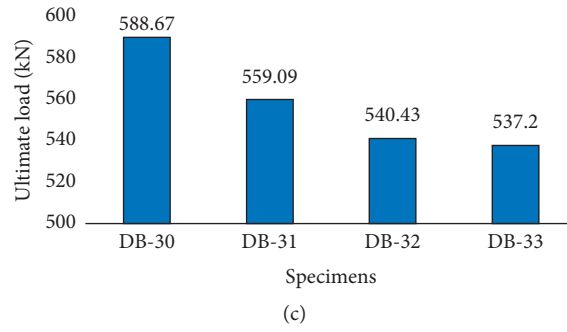

FIGURE 16: Continued.

(c)

FIGURE 16: Load-carrying capacity comparison under different L/R ratios. (a) Beam with L/D ratio equal to 3, (b) beam with L/D ratio equal to 2.67, and (c) beam with L/D ratio equal to 2.4.

TABLE 6: Summary of outputs from FE simulation.

| Beam ID	At first cracking			At ultimate		
	Pcr (kN)	Δcr (mm)	θcrx10e-3 radian	Pult (kN)	Δult (mm)	θultx10e-3 radian
DB10	185.72	1.702	0.000	424.15	6.490	0.000
DB11	178.41	1.711	3.691	416.51	6.869	55.06
DB12	170.06	1.759	4.220	405.21	7.210	60.48
DB13	163.47	1.845	4.320	399.92	7.614	62.56
DB20	221.70	1.407	0.000	503.29	5.193	0.000
DB21	211.14	1.472	2.818	489.20	5.386	37.07
DB22	202.64	1.505	3.003	481.69	5.611	39.72
DB23	194.33	1.531	2.810	471.36	5.944	43.61
DB30	249.11	1.426	0.000	588.67	4.660	0.000
DB31	239.51	1.435	2.183	559.09	4.927	28.46
DB32	230.68	1.392	2.375	543.43	5.300	31.35
DB33	221.40	1.433	2.342	537.20	5.626	34.36
DB11-L	196.82	1.515	3.077	480.06	6.498	52.26
DB13-L	183.58	1.706	4.134	447.75	7.287	59.66
DB11-S	186.62	1.581	3.113	455.16	6.573	52.87
DB13-S	175.41	1.752	4.177	427.82	7.363	60.28

(a)

(b)
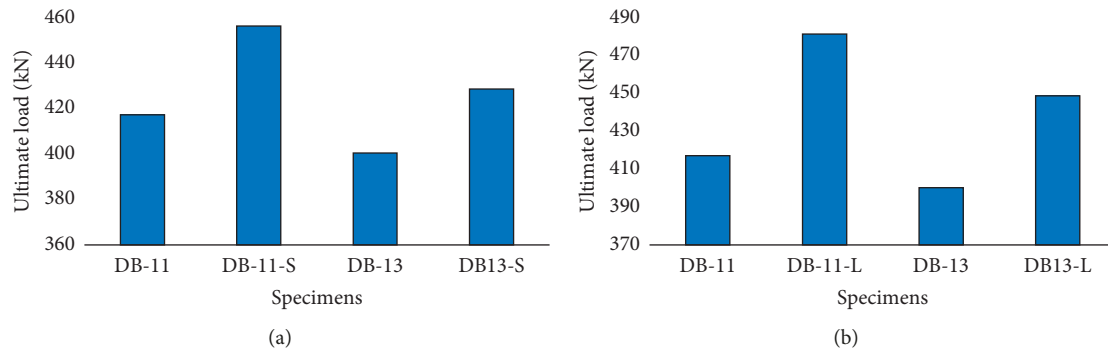
FIGURE 17: Ultimate load capacity of beam specimens with different. (a) Vertical shear reinforcement spacing and (b) longitudinal steel ratio.

4. Conclusion

In this study, the numerical FE simulation was conducted to investigate the behavior of curved beams, using L/D ratio, L/R ratio, longitudinal reinforcement ratio, and spacing of vertical shear reinforcement as study parameters within Abaqus/CAE finite element software. The study revealed the significant effect of the study parameters on the load capacity of the beams. The load-carrying capacity of the beam decreased up to 27.95%, as the L/D ratio increased from 2.4 to 3. In addition, as the L/R ratio increased from 0 to 1.57, the load-carrying capacity decreased up to 8.74%. Furthermore, as the longitudinal reinforcement ratio increased from 0.02042 to 0.02608 and the spacing shear reinforcement decreased from 100 mm to 50 mm, the load-carrying capacity increased up to 9.28% and 4.3%, respectively. The increase in the L/R ratio resulted in the development of internal torsion in structural beam elements, which in turn caused the decrease in ultimate load capacity. The 3D nonlinear finite element model adopted is suitable to predict the load-carrying capacity of the beams in particular and to evaluate the behavior of the deep beam in general. The numerical results are in good agreement with available experimental results. Furthermore, sensitivity analysis was performed based on the result obtained from the FE simulation.

Data Availability

All required data were included in the manuscript.

Conflicts of Interest

The author has no conflicts of interest to disclose.

Acknowledgments

References

[1] A. H. Nilson, D. Darwin, and C. W. Dolan, *Design of Concrete Structures*, McGraw-Hill Companies, Inc, New York, NY, USA, 14th edition, 2009.

[2] IS-456, *Plain and Reinforced Concrete- Code of Practice*, Bureau of Indian Standards, Delhi, India, 4th edition, 2000.

[3] ACI Committee 318, *Building Code Requirements for Structural Concrete*, ACI, Hills, MI, USA, 2014.

[4] EBCS2, *Structural use of concrete*, WordPress, San Francisco, CA, USA, 1995.

[5] S. M. Islam and A. Khennane, "Experimental verification of automated design of reinforced concrete deep beams," *SIMULIA Customer*, pp. 978–981, 2012.

[6] K. S. Abdul-Razzaq, A. M. Jalil, and S. F. Jebur, "Behaviour of reinforced concrete deep beams in previous studies," *IOP Conference Series: Materials Science and Engineering*, vol. 518, no. 2, Article ID 022065, 2019.

[7] M. Shariat, H. Eskandari-Naddaf, M. Tayyebinia, and M. Sadeghian, "Sensitivity analysis of reinforced concrete deep beam by STM and FEM (Part III)," *Materials Today Proceedings*, vol. 5, no. 2, pp. 5529–5535, 2018.

[8] K. H. Tan, K. Tong, and C. Y. Tang, "Consistent strut-and-tie modelling of deep beams with web openings," *Magazine of Concrete Research*, vol. 55, no. 1, pp. 65–75, 2003.

[9] N. Nair and P. E. Kavitha, "Effect of openings in deep beams using strut and tie model method," *International Journal of Technical Research and Application*, vol. 3, pp. 59–62, 2015.

[10] J. I. Enem, J. C. Ezeh, M. S. W. Mbagiorgu, and D. O. Onwuka, "Analysis of deep beam using finite element method," *International Journal of Applied Science and Engineering Research*, vol. 1, no. 2, pp. 348–356, 2012.

[11] A. A. Kusanale, P. S. B. Kadam, and S. N. Tande, "Analysis and design of R. C. Deep beam by finite element method," *International Journal of Emerging Engineering Research and Technology*, vol. 2, no. 4, pp. 166–169, 2014.

[12] A. M. Halahla, "Study the behavior of reinforced concrete beam using Finite Element Analysis," in *Proceedings of the 5th World Congress on Civil, Structural, and Environmental Engineering*, Budapest, Hungary, 2018.

[13] ABAQUS, *Abaqus 6.14*, ABAQUS, Providence, RI, USA, 2014.

[14] I. M. Metwally, "Three-dimensional nonlinear finite element analysis of concrete deep beam reinforced with GFRP bars," *HBRC Journal*, vol. 13, no. 1, pp. 25–38, 2017.

[15] Y. J. Lafta and K. Ye, "Structural behavior of deep reinforced concrete beams under indirect loading condition," *International Journal of Civil, Structural, Environmental and Infrastructure Engineering Research and Development*, vol. 5, no. 4, pp. 53–72, 2015.

[16] A. Y. Ali and M. G. Zghair, "Experimental investigation and nonlinear analysis of hybrid reinforced concrete deep beams," *Al-Qadisiyah Journal in Engineering Sciences*, vol. 8, no. 2, pp. 99–119, 2015.

[17] S. A. Kedge, U. H. Momin, and M. V Nagendra, "Experimental analysis of deep beam strengthened by glass fiber reinforced polymer plate," *International Research Journal of Engineering and Technology*, vol. 5, 2018.

[18] B. Isojeh, M. El-Zeghayar, and F. J. Vecchio, "High-cycle fatigue life prediction of reinforced concrete deep beams," *Engineering Structures*, vol. 150, pp. 12–24, 2017.

[19] A. A. Al-Azzawi and A. S. Shaker, "Finite difference analysis of curved deep beams on Winkler foundation," *Journal of Engineering and Applied Sciences*, vol. 6, no. 3, pp. 42–48, 2011.

[20] European Committee for Standardization, Eurocode 2: Design of concrete Structures - Part 1: General Rules and Rules for buildings November, vol. 1, European Committee for Standardization, Brussels, Belgium, 2002.

[21] Y. Sümer and M. Aktaş, "Defining parameters for concrete damage plasticity model," *Challenge Journal of structural Mechanics*, vol. 1, no. 3, pp. 149–155, 2015.

[22] A. Hamicha and G. Kenea, "Investigation on the effect of geometric parameter on reinforced concrete exterior shear wall-slab connection using finite element analysis," *Advances in Civil Engineering*, vol. 2022, Article ID 4903650, 17 pages, 2022.

[23] E. Megarsa and G. Kenea, "Numerical investigation on shear performance of reinforced concrete beam by using ferrocement composite," *Mathematical Problems in Engineering*, vol. 2022, Article ID 5984177, 12 pages, 2022.

[24] T. Wang and T. T. C. Hsu, "Nonlinear finite element analysis of concrete structures using new constitutive models," *Computers & Structures*, vol. 79, no. 32, pp. 2781–2791, 2001.

[25] R. Malm, G. S. James, and Hakan, "Monitoring and evaluation of shear crack initiation and propagation in webs of concrete

box-girder sections," in *Proceedings of the International Conference on Bridge Engineering—Challenges in the 21st Century*, Hong Kong, China, 2003.

[26] J. Lee, G. L. Fenves, and M. Asce, "Plastic-damage model for cyclic loading of concrete structures," *Journal of Engineering Mechanics*, vol. 124, no. 8, pp. 892–900, 1998.

[27] W. Ren, L. H. Sneed, Y. Yang, and R. He, "Numerical simulation of prestressed precast concrete bridge deck panels using damage plasticity model," *International Journal of Concrete Structures and Materials*, vol. 9, no. 1, pp. 45–54, 2015.

[28] H. Kupfer, H. Hilsdorf, and H. Rusch, "Behaviour of concrete under biaxial stresses," *International Concrete Abstracts Portal*, vol. 66, no. 8, pp. 656–666, 1969.

[29] J. Lubliner, J. Oliver, S. Oller, and E. Onate, "A plastic-damage model for concrete," *International Journal of Solids and Structures*, vol. 25, no. 3, pp. 299–326, 1989.

[30] A. Feyissa and G. Kenea, "Performance of shear connector in composite slab and steel beam with reentrant and open trough profiled steel sheeting," *Advances in Civil Engineering*, vol. 2022, Article ID 5010501, 14 pages, 2022.

[31] A. A. Al-Manaseer and D. V. Phillips, "Numerical study of some post-cracking material parameters affecting nonlinear solutions in RC deep beams," *Canadian Journal of Civil Engineering*, vol. 14, no. 5, pp. 655–666, 1987.

[32] I. J. Jordaan, M. M. A. Khalifa, and A. E. McMullen, "Collapse of curved reinforced concrete beams," *Journal of the Structural Division*, vol. 100, no. 11, pp. 2255–2269, 1974.